Dynamic behavior of stall fluttering airfoils

Luiz G. P. dos Santos, Dinâmica e Mecatrônica, luizpancini@usp.br
Flávio D. Marques, Dinâmica e Mecatrônica, fmarques@sc.usp.br

Abstract. *Stall flutter is turning into a more likely condition to be encountered as the demand for increasingly more flexible wings grows for HALE-like aircraft. Due to the various nonlinearities involved that can lead to complex motion, the characterization of the dynamical behavior in the post-flutter condition becomes important. The dynamics of a pitch-plunge idealized HALE typical section with aerodynamic, structural and kinematic nonlinearities in the stall flutter regime was investigated using an aeroelastic state-space formulation which includes a modified Beddoes-Leishman dynamic stall model. The results reveal that period-doubling was possible without stall, but chaos arose at discontinuity-induced bifurcations due to dynamic stall.*

Keywords: *Piecewise-smooth systems. Discontinuity-induced bifurcations. Chaos. Dynamic stall. HALE*

1. INTRODUCTION

Current engineering designs are pushing the limits towards high-span, flexible wings, such as those of HALE (High-Altitude-Long-Endurance) aircraft, helicopter and wind turbine blades. Because of the operational conditions and structural flexibility of these machines, it is likely they will at some point encounter stall flutter, a highly nonlinear aeroelastic phenomenon of self-sustained oscillations, in which the wing is stalled during part of each cycle. These limit-cycle oscillations (LCOs) are part favorable, part unfavorable. The fact that they bound the response above the flutter speed, which is usually considered a stability limit for flight vehicles, is a positive outcome. However, structural fatigue, decreased performance and control difficulties are adverse issues. HALE and other Unmanned Aerial Vehicles (UAVs), for instance, may fly near their stability limits in order to maximize performance. This increases the chances of a disturbance prompting an undesirable dynamical response. Therefore, it becomes of primary importance to characterize the post-flutter aeroelastic behavior of such machines, assessing dangerous bifurcations and the possibility of chaos development. Even though previous studies (Patil and Hodges, 2006; Su and Cesnik, 2011) have shown that the coupling of aeroelasticity and flight dynamics is mandatory to analyze the behavior of very flexible aircraft like HALE, a simplified analysis like the present one can be quite insightful from the aeroelastic perspective, more so due to the greater realism of aerodynamic nonlinearities considered here, *i.e.*, dynamic stall.

This so-called dynamic stall, upon which stall flutter is established, is a very complex fluid phenomenon and consequently is extremely difficult to model. The most precise representations of the phenomenon are experimental, but it is virtually impossible to rely solely on experiments in order to harness aerodynamic data for every combination of flow and motion condition. Despite of these difficulties, many low-fidelity semi-empirical models with reasonable accuracy have been developed for 2D flows at harmonic motion, with the intention of being used at the preliminary design stages, when a vast number of candidate solutions must be evaluated. Either for helicopter, fixed-wing or wind turbine applications, the Beddoes-Leishman (Leishman and Beddoes, 1986) model and its modified versions are among the most popular. It can be represented in a state-space formulation that may easily be fitted in an aeroelastic framework when joined to the equations of motion. Although dynamic stall nonlinearities can play a determinant role in the aeroelastic stability of flexible wings, not many researchers have appreciated its due importance.

The present work investigates the bifurcations and post-flutter dynamics of a low-fidelity autonomous aeroelastic model of an airfoil representative of HALE aircraft, undergoing stall flutter self-sustained oscillations. The structural model is reduced to only two degrees of freedom, pitch and plunge, with a kinematically-exact approach that is more adequate for the high angles of attack involved. Special modeling emphasis is given to aerodynamic nonlinearities, which are handled by a modified Beddoes-Leishman dynamic stall model. The dynamics are henceforth analyzed through bifurcation diagrams and frequency spectra, revealing an overall picture of the behavior of the system. The objective is to develop a methodology suitable for initial estimations of post-flutter aeroelastic stability.

2. METHODOLOGY

The unsteady aerodynamic loading prediction is performed with a semi-empirical approach based on the Beddoes-Leishman model in state space, following Leishman and Crouse Jr. (1989). The model was chosen because its equations are derived in a physics-based approach and facilitate augmentations. The typical aeroelastic section receives these airloads, thereby allowing time integration of the equations of motion. The complete system is piecewise-smooth with a kind of fixed-time intermittent forcing, so the necessary precautions are exercised in the numerical procedures.

2.1 Equations of motion

The definition of parameters of the 2-DOF typical section follows in Tab. (1), and illustrated in Fig. (1).

Table 1: Reference typical section parameters.

Parameter [unit]	Value	Description
α_I [deg]	4	Wind-off angle of attack
γ_α	0.5	Cubic pitch stiffness coefficient
γ_h	0.5	Cubic plunge stiffness coefficient
$\mu = m/\pi\rho b$	30	Mass ratio
ρ [kg/m^3]	0.0880	Freestream air density
$\omega_\alpha = \sqrt{K_\alpha/I_\alpha}$ [rad/s]	15.5	Pitch natural frequency
$\omega_h = \sqrt{K_h/m}$ [rad/s]	3.1	Plunge natural frequency
$\bar{\omega} = \omega_h/\omega_\alpha$	0.2	Frequency ratio
a_∞ [m/s]	295.1	Freestream sound speed
a_h	-0.4	Elastic axis (EA) semichords after midchord
b [m]	1	Semichord
C_α	$K_\alpha/100$	Pitch damping coefficient
C_h	$K_h/100$	Plunge damping coefficient
H [km]	20	Altitude
$r_\alpha = \sqrt{I_\alpha/mb^2}$	0.5	Radius of gyration, in semichords
x_α	0.3	Center of gravity (CG) semichords after EA

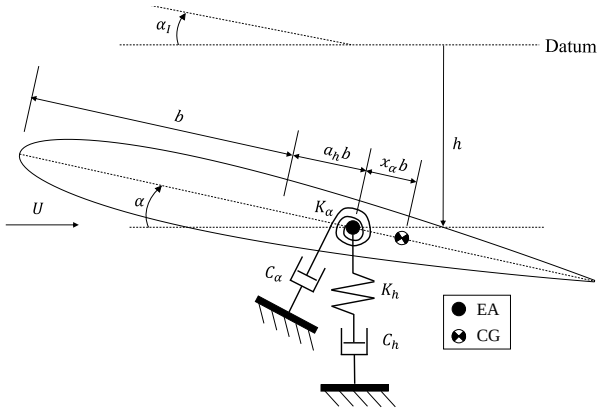

Figure 1: Typical section geometry.

The kinematically-exact equations of motion are derived from Euler-Lagrange's equations as

$$\begin{aligned} m\ddot{h} + S_\alpha\ddot{\alpha}\cos\alpha - S_\alpha\dot{\alpha}^2\sin\alpha + C_h\dot{h} + K_h\left(h + \gamma_h h^3\right) &= -\rho b U^2 c_l \\ S_\alpha\ddot{h}\cos\alpha + I_\alpha\ddot{\alpha} + C_\alpha\dot{\alpha} + K_\alpha\left[(\alpha - \alpha_I) + \gamma_\alpha(\alpha - \alpha_I)^3\right] &= 2\rho b^2 U^2 c_{m_{ea}} \end{aligned} \tag{1}$$

where α is the geometric pitch angle and h is the plunge displacement, m is the airfoil's mass per unit length, K_α and K_h are the stiffness coefficients, $S_\alpha = mbx_\alpha$ and I_α are the first and second moments of inertia about the EA, U is the

freestream airspeed, and c_n, c_c, $c_l = (c_n \cos\alpha + c_c \sin\alpha)$ and $c_{m_{ea}} = c_m + (1/4 + a_h/2)c_n$ are respectively the normal, chordwise, lift, and pitching moment coefficient at the EA (c_m is the pitching moment coefficient at the quarter-chord).

2.2 Dynamic stall model

The Beddoes-Leishman model can be broken down into four modules, ***(i)*** unsteady attached flow loading; ***(ii)*** stall onset determination; ***(iii)*** trailing edge separation effects; ***(iv)*** and leading-edge vortex shedding. The total airloads are given by contributions of each module, so that $c_n = c_n^f + c_n^I + c_n^v$, $c_c = c_c^f$ and $c_m = c_m^f + c_m^I + c_m^v$. A formulation for these coefficients similar to the one employed in the present work can be found in dos Santos and Marques (2021). When inserted back into Eq. (1), they complete the state-space model, which can be expressed as

$$\dot{\boldsymbol{x}} = \boldsymbol{f}(\boldsymbol{x},\ \dot{\boldsymbol{x}}) \tag{2}$$

where $\boldsymbol{x}$ is the vector of 12 states, $\dot{\boldsymbol{x}}$ is its derivative and $\boldsymbol{f}(\boldsymbol{x},\ \dot{\boldsymbol{x}})$ is the corresponding vector of nonlinear equations, integrated in time with a Runge-Kutta-Fehlberg algorithm. A validation of the model through comparison with the experimental data published by McAlister et al. (1982) is presented in Fig. (2).

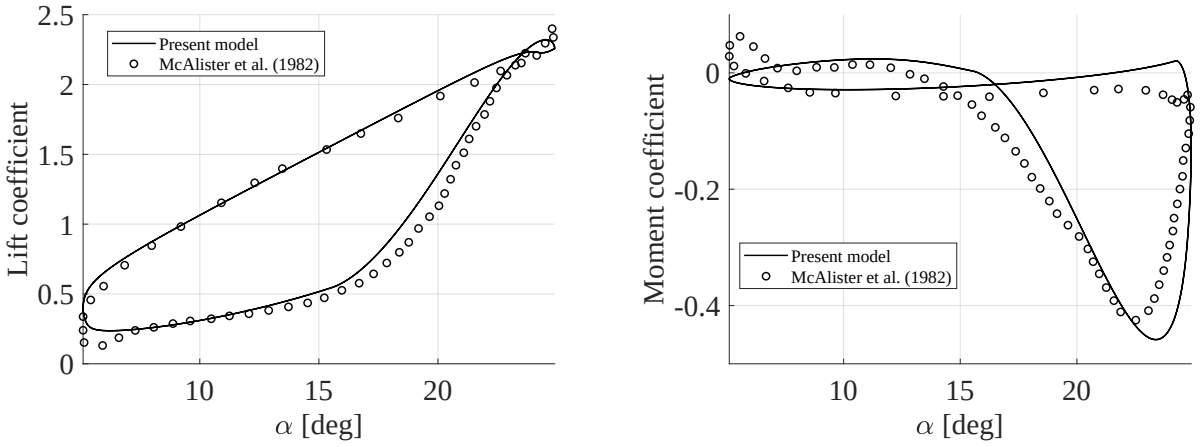

Figure 2: Dynamic stall aerodynamic coefficients at $M = U/a_\infty = 0.072$ and $k = \omega b/U = 0.25$ - deep stall regime.

3. RESULTS

To characterize the post-flutter behavior, the linear flutter condition (Hopf point) had to be identified first, by solving for its fixed-point (setting Eq. (2) equal to zero) with a Newton-Raphson algorithm, and assessing the corresponding eigenvalues of the Jacobian matrix. This analysis yielded a flutter speed $U_F \approx 42.65$ m/s ($M_F \approx 0.145$) and a flutter frequency of $\omega_F \approx 1.36$ Hz ($k_F \approx 0.20$). With the Hopf point at hand, the numerical continuation scheme with a shooting method could be started, as well as the simulations for investigation of the post-flutter behavior. The bifurcation diagram in Fig. (3) depicts the local extrema of the pitch variables (α_A) with the evolution of the airspeed ratio U/U_F, as obtained through the direct numerical simulations (DNS). The airspeed was slowly varied until transients died out and the values were gathered for 60 seconds of oscillations. Also are shown the global extrema values according to the shooting method (SM) in some regions, being in perfect agreement with the time simulations. The loci of the unstable focus is included for reference as well. From the outset, it was determined that the range of interest for this study would be for $U/U_F \leq 1.2$, or until a maximum effective angle of attack of $45°$ was reached, in order not to go too far beyond the limits validated for the dynamic stall model.

It can be seen in the diagram that the Hopf bifurcation is supercritical, and that a branch of periodic solutions grows in amplitude until $U = U_{PD} = 1.0594U_F$. At this point, a supercritical period-doubling bifurcation occurs, as suggested by the appearance of two local maxima and two local minima. These period-doubled oscillations occur without the presence of dynamic stall during the entire cycle, and no leading-edge vortex is shed. From an analysis of the state space variables, it could be concluded that this bifurcation was not associated with the crossing of any discontinuity boundaries. Period-2 (P-2) motion continues like so until $U = U_c = 1.0635U_F$, when finally dynamic stall begins, the orbit undergoes a discontinuity-induced bifurcation known as boundary-crossing (BC) (di Bernardo et al., 2008), and the solution transitions into chaos. It develops through intermittency, given that the closer to U_c, the longer the stretches of time around the "ghost"

period-2 orbit, as illustrated in the upper corner time history right at U_c. As a consequence, no hysteresis is observed by changing U around U_c. A window of chaotic oscillations is present in the range $1.0635 \leq U/U_F \leq 1.089$, and it is seen that local extrema develop in four separate bands. As shown in the lower zoomed-in window, at $U/U_F \approx 1.089$, the chaotic solution ceases and two stable attractors co-exist, one in a period-4 (P-4), and other in a period-2 orbit. The former has a wider basin of attraction and is more stable, thus being realized as the airspeed is slowly increased or decreased in this region. The amplitude difference between the peaks of this period-4 branch rapidly shrinks around $U/U_F \approx 1.095$, and then only the period-2 solutions are possible. There is no evidence that at this point the system undergoes a reverse supercritical period-doubling bifurcation (a "period-halving"), but instead that the period-4 orbit gives way to the period-2 due to synchronizations between vortex-shedding and structural frequencies. The part of the stable period-2 branch that co-exists with both the period-4 and chaotic orbits in the range of $1.083 \leq U/U_F \leq 1.095$ is less stable and cannot be easily realized in the direct numerical simulations. Following its branch in the direction of decreasing airspeed, it is seen that at $U/U_F \approx 1.083$ it suffers a period-doubling bifurcation, as indicated in the lower zoomed-in window of the diagram, and at $U/U_F \approx 1.0697$, one of the Floquet multipliers becomes highly negative and the shooting algorithm cannot converge due to the high instability. In the direction of increasing airspeed, the stable period-2 solutions are sustained until $U/U_F \approx 1.1808$, when the numerical solutions jump to another branch, in which the airfoil now undergoes dynamic stall under both positive and negative angles of attack (P/N DSVs), with vortex airloads overlapping during part of the cycle. The shooting method allowed the characterization of this dangerous bifurcation as a cyclic fold, indicated by the direction vector of the continuation parameter (U) changing sign. Solutions on this new branch continue well beyond $U/U_F = 1.2$, but if the airspeed is slowly decreased, the simulations show that this branch remains stable down to $U/U_F \approx 1.158$, when another cyclic fold takes place, thus causing a hysteresis effect. Although the unstable branches emanating from the folds were not located with the shooting method due to the high computational cost for convergence in this region ($\mathcal{O}(\Delta t_{\max}) = 10^{-6}$) and also the presence of highly unstable Floquet multipliers, it is quite possible that they are in fact only one branch, undergoing a double cyclic fold.

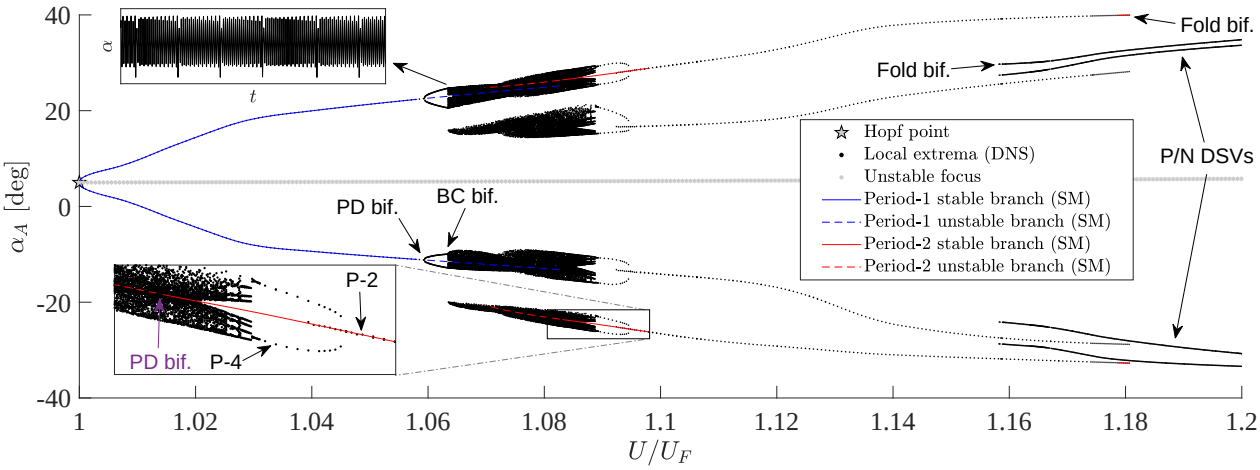

Figure 3: Pitch bifurcation diagram.

By evaluating the frequency content of the solutions, further insights on the behavior of the system can be gained. Fig. (4) contains the spectrograms of the pitch and nondimensional plunge ($\xi = h/b$) variables across the entire range of airspeed, as it is slowly increased from U_F. The simulations from Fig. (3) were continued for more 120 seconds, yielding a frequency resolution of $1/120 \approx 0.0083$ Hz in the spectra. Just after the Hopf bifurcation, it can be noticed that the prevalent frequency of motion is the plunge one (ω_ξ), which is equal to the flutter frequency (ω_F) at that point. The presence of quadratic and cubic nonlinearities is clear from the smaller peaks at both even and odd superharmonics, whose effects on the periodic solution grow steadily until $U = U_{PD}$. The strongest nonlinearities in this range of periodic solutions are due to structural damping and hardening, while the aerodynamic ones related to small trailing-edge separation and nonlinear kinematics are present only to a very limited degree. The pitch frequency does not appear to play any role so far. As the period-doubling bifurcation takes place, the 1/2 plunge subharmonic ($1/2\ \omega_\xi$) suddenly appears, along with other ultrasubharmonics ($n + 1/2\ \omega_\xi, n$ integer). Increasing the airspeed to $U = U_c$, chaos develops at the BC bifurcation, as is clear from the broadband character of the spectra. Inside the chaotic window, the pitch spectrum reveals stronger influence of frequencies in the range $1 < \omega/\omega_F < 2$, while the plunge spectrum is more "noisy" for frequencies in the range $1/2 < \omega/\omega_F < 1$. After chaos is suppressed, the presence of the 1/4 plunge subharmonic ($1/4\ \omega_\xi$) and its related ultrasubharmonics ($n + 1/4\ \omega_\xi, n$ integer) is evident, in accordance with the observed period-4 orbit. The dynamic

stall vortices' (DSV) intermittent forcing raises the possibility of resonances if the vortex-shedding frequency, ω_{DSV}, synchronizes with other frequencies of motion, or rational fractions of them, which is exactly what happens in the present case. During the period-4 oscillations, two unequal vortices are shed per cycle, each at a frequency ω_{DSV} which is half the fundamental one, ω_ξ. The overall effect is that of a superharmonic resonance of order 4. As the airspeed is increased further, the phase difference between the shedding of the two vortices' gradually reduces, resulting in the period-2 orbit. It is also noted that after the chaotic oscillations, the dominant frequency in the plunge spectrum is the subharmonic of $1/2\ \omega_\xi = \omega_{DSV}$. On the other hand, the pitch spectrum remains dominated by the ω_ξ frequency, but also with strong influences from the $1/2\ \omega_\xi$ subharmonic. Moreover, it is remarked that even after dynamic stall sets in, the motion is still dominated by the plunge mode. This is in contrast with previous observations of stall flutter in pitch-plunge wings (Razak et al., 2011; Poirel et al., 2018), in which the leading mode was reported to be the pitch one. As the airspeed is raised, all of the frequencies also do so, as indicated by the continuous "bending" of the peaks to the right in the plots. Finally, for $U/U_F \gtrapprox 1.18$, the peaks are suddenly shifted to the right, as they reflect solutions on the other attractor discussed in Fig. (3), in which dynamic stall occurs at positive and negative angles of attack. Now the motion is dominated by the pitch frequency ($\omega_\alpha \approx 1.63\omega_F$, which in this context must not to be confused with the fixed value given in Tab. (1)), and its subharmonic, which resonates with the vortex frequency ($1/2\ \omega_\alpha = \omega_{DSV}$). Therefore, solutions on this branch are also period-doubled.

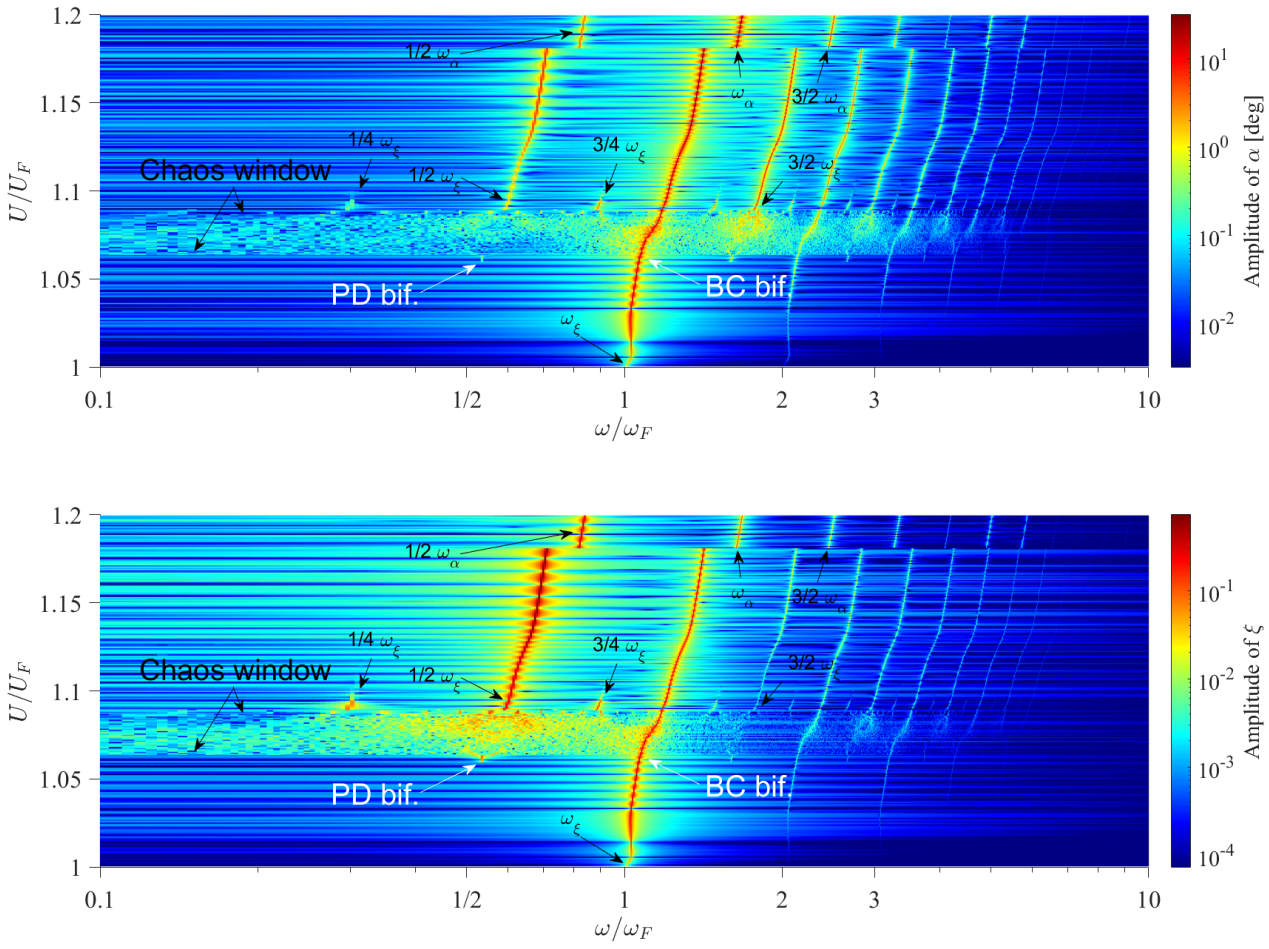

Figure 4: Spectrograms.

4. CONCLUSIONS

This study has investigated the post-flutter, stall fluttering behavior of a pitch-plunge typical section representative of HALE aircraft, at a reference altitude of 20 km, which is common for these vehicles. An appropriate non-smooth dynamic stall model has been employed to capture aerodynamic nonlinearities, accompanied by simplified structural hardening and

damping. Analysis methods appropriate for discontinuous systems were adopted. Some key concluding remarks can be drawn from this study, while the dynamic stall model limitations, and the limited range of parameters investigated should be kept in mind:

1. For the present model, the general mechanism of evolution of solutions is through period-doubling bifurcations, which can take place even before the onset of dynamic stall and stall flutter *per se*. However, as stall flutter begins, it is possible that resonances occur due to the interaction between structural and vortex-shedding frequencies, leading to high-period motion. These frequencies may lock-in, or synchronize, for a considerable range of airspeeds, and with several vortices being shed at each cycle.

2. The occurrence of dynamic stall (and therefore stall flutter) has lead to a boundary-crossing bifurcation and coincidentally, chaos development. Given that dynamic stall cycles are experimentally observed to be non-repeatable, *i.e.*, intrinsically aperiodic, appropriate methods would have to be employed in an experimental setting to identify possibly periodic solutions of stall fluttering airfoils.

While the present methodology as a whole seems promising for post-flutter analyses due to the relatively low computational cost, it still requires a strict validation with high-fidelity (CSD-CFD) or experimental methods.

5. REFERENCES

di Bernardo, M.; Budd, C. J.; Champneys, A. R.; Kowalczyk, P. *Piecewise-smooth dynamical systems: theory and applications*. Springer Science & Business Media, 2008.

dos Santos, L. G. P.; Marques, F. D. Nonlinear aeroelastic analysis of airfoil section under stall flutter oscillations and gust loads. *Journal of Fluids and Structures*, 102:103250, 2021. doi: 10.1016/j.jfluidstructs.2021.103250.

Leishman, J. G.; Beddoes, T. S. A generalised model for airfoil unsteady aerodynamic behaviour and dynamic stall using the indicial method. In *Proceedings of the 42nd Annual forum of the American Helicopter Society*, pages 243–265. Washington, DC, 1986.

Leishman, J. G.; Crouse Jr, G. L. State-space model for unsteady airfoil behavior and dynamic stall. In *30th Structures, Structural Dynamics and Materials Conference*, pages 1372–1383, 1989. doi: 10.2514/6.1989-1319.

McAlister, K. W.; Pucci, S. L; McCroskey, W. J.; Carr, L. W. An experimental study of dynamic stall on advanced airfoil section. Volume 2: pressure and force data. Technical memorandum, NASA-TM-84245, 1982. URL `https://ntrs.nasa.gov/archive/nasa/casi.ntrs.nasa.gov/19830003778.pdf`.

Patil, M. J.; Hodges, D. H. Flight dynamics of highly flexible flying wings. *Journal of Aircraft*, 43(6):1790–1799, 2006. doi: 10.2514/1.17640.

Poirel, D.; Goyaniuk, L.; Benaissa, A. Frequency lock-in in pitch–heave stall flutter. *Journal of Fluids and Structures*, 79: 14–25, 2018. doi: 10.1016/j.jfluidstructs.2018.01.006.

Razak, N. A; Andrianne, T.; Dimitriadis, G. Flutter and stall flutter of a rectangular wing in a wind tunnel. *AIAA Journal*, 49(10):2258–2271, 2011. doi: 10.2514/1.J051041.

Su, W.; Cesnik, C. E. S. Dynamic response of highly flexible flying wings. *AIAA Journal*, 49(2):324–339, 2011. doi: 10.2514/1.J050496.

6. ACKNOWLEDGEMENTS

The authors acknowledge the financial support of the National Council for Scientific and Technological Development – CNPq (grants #132154/2019-6 and #306824/2019-1) and São Paulo State Research Agency – FAPESP (grant #2017/02926-9).

7. DISCLAIMER

The authors are the only ones responsible for the information included in this work.